Network subgraph-based approach for analyzing and comparing molecular networks

Chien-Hung Huang[1,*], Efendi Zaenudin[2,3], Jeffrey J.P. Tsai[3], Nilubon Kurubanjerdjit[4] and Ka-Lok Ng[3,5,6,*]

[1] Department of Computer Science and Information Engineering, National Formosa University, Yun-Lin, Taiwan
[2] National Research and Innovation Agency, Bandung, Jawa Barat, Republic of Indonesia
[3] Department of Bioinformatics and Medical Engineering, Asia University, Taichung, Taiwan
[4] School of Information Technology, Mae Fah Luang University, Chiang Rai, Thailand
[5] Center for Artificial Intelligence and Precision Medicine Research, Asia University, Taichung, Taiwan
[6] Department of Medical Research, China Medical University Hospital, China Medical University, Taichung, Taiwan
[*] These authors contributed equally to this work.

ABSTRACT

Molecular networks are built up from genetic elements that exhibit feedback interactions. Here, we studied the problem of measuring the similarity of directed networks by proposing a novel alignment-free approach: the network subgraph-based approach. Our approach does not make use of randomized networks to determine modular patterns embedded in a network, and this method differs from the network motif and graphlet methods. Network similarity was quantified by gauging the difference between the subgraph frequency distributions of two networks using Jensen–Shannon entropy. We applied the subgraph approach to study three types of molecular networks, *i.e.*, cancer networks, signal transduction networks, and cellular process networks, which exhibit diverse molecular functions. We compared the performance of our subgraph detection algorithm with other algorithms, and the results were consistent, but other algorithms could not address the issue of subgraphs/motifs embedded within a subgraph/motif. To evaluate the effectiveness of the subgraph-based method, we applied the method along with the Jensen–Shannon entropy to classify six network models, and it achieves a 100% accuracy of classification. The proposed information-theoretic approach allows us to determine the structural similarity of two networks regardless of node identity and network size. We demonstrated the effectiveness of the subgraph approach to cluster molecular networks that exhibit similar regulatory interaction topologies. As an illustration, our method can identify (i) common subgraph-mediated signal transduction and/or cellular processes in AML and pancreatic cancer, and (ii) scaffold proteins in gastric cancer and hepatocellular carcinoma; thus, the results suggested that there are common regulation modules for cancer formation. We also found that the underlying substructures of the molecular networks are dominated by irreducible subgraphs; this feature is valid for the three classes of molecular networks we studied. The subgraph-based approach provides a systematic scenario for analyzing, compare and classifying molecular networks with diverse functionalities.

Submitted 19 July 2021
Accepted 28 February 2022
Published 3 May 2022

Corresponding author
Ka-Lok Ng, ppiddi@gmail.com

Academic editor
Shawn Gomez

Additional Information and Declarations can be found on page 24

DOI **10.7717/peerj.13137**

How to cite this article Huang C-H, Zaenudin E, Tsai JJP, Kurubanjerdjit N, Ng K-L. 2022. Network subgraph-based approach for analyzing and comparing molecular networks. *PeerJ* **10**:e13137 http://doi.org/10.7717/peerj.13137

Subjects Bioinformatics, Computational Biology, Molecular Biology
Keywords Network subgraphs, Cancer networks, Signal transduction networks, Cellular processes, Graph theory, Information theory, Entropy, Jensen-Shannon entropy

INTRODUCTION

Network comparison is an important and well-studied subject in bioinformatics. Many molecular biology networks are directed networks (digraphs), such as gene regulatory networks, signal transduction networks, cellular processes, metabolic networks etc. In the area of computational molecular biology, it is useful to compare networks with each other, because if the properties of a given network are known, one can transfer this information to the other network; such as, structural study of metabolic networks for single cell organism (*Zhu & Qin, 2005*), inferring phylogenetic tree for metabolic networks (*Heymans & Singh, 2003*), grouping different types networks; such as, cell signaling, metabolic and transcriptional regulatory networks (*Aparìcio, Ribeiro & Silva, 2015*).

Alignment-based methods and alignment-free methods

Alignment-based methods are mainly used to compare whether the nodes and edges of two networks are similar, and to identify conserved modules. Alignment-free methods do not need to consider the node identity and network size, so they may not find conserved regions (*Yaveroğlu, Milenković & Pržulj, 2015*); instead, the methods can extract conserved topological similar regions.

There are a few methods that can be used to analyze digraphs (*Tantardini et al., 2019*); including (i) global statistics (*Pržulj, 2007*), (ii) portrait divergence (PD) (*Bagrow & Bollt, 2019*), (iii) graphlet (*Sarajlić et al., 2016*) and (iv) algorithmic complexity of network motifs (*Zenil, Kiani & Tegnér, 2013*). Methods (i) to (iii) use graph theory metrics, whereas (iv) uses information contents of the motifs to compare networks. Each method has its advantages and limitations.

Networks with similar global statistics do not necessary mean similar network architecture (*Pržulj, 2007*). The PD method defines three probability distributions to characterize a graph: (i) the probability that two points in the network are connected, (ii) the probability that the distance between the two nodes is L, and (iii) the probability that one of the nodes is connected to a k-1 nodes at a distance of L. Then, the graph invariant (the network portrait) is defined by taking the normalized product of these three probability distributions. Level of network similarity is given by the Jensen–Shannon entropy (H_{JS}) of the two network portraits. The authors demonstrated that their method was able to distinguish the protein interaction, neuroscience, and social science networks, but only a few networks are considered.

The use of graphlets was introduced by Przulj to perform network comparisons (*Przulj, 2007*; *Yaveroglu et al., 2014*). Graphlets are connected small graphs. Each node in the graphlet can be divided into different categories depending on its connection to other nodes in the network. Nodes in the same category belong to the same orbit. To study directed networks, the concept of the graphlet was extended to directed graphlets by considering the in- and out-degree. Directed graphlets were demonstrated to be superior

for comparing directed networks (*Sarajlić et al., 2016*) and effective in studying brain networks (*Trpevski et al., 2016*). The graphlet method compares two directed networks by decompose the network into three-node and four-node graphlets, and calculate the Euclidean distance between their Directed Graphlet Correlation Matrix (*Sarajlić et al., 2016*). *Sarajlić et al. (2016)* applied the directed graphlet degree concept to predict the biological function of enzymes according to the similarity of their connection patterns in a metabolic network. *Trpevski et al. (2016)* analyzed the brain network by using the (i) signature vector of the vertex (brain region) and (ii) graphlet correlation matrix of the network to infer the excitatory/inhibitory and causal patterns, respectively, in the effective brain networks.

New methods have been developed to perform directed network comparisons, including expanding the definition of graphlets (*Martin et al., 2016*) and using graphlet-based metrics (GBM) (*Martin et al., 2017*). *Martin et al. (2016)* introduced the rate of graphlet reconstruction and REC graphlet degree (RGD) to compare gene regulatory networks (from *Escherichia coli*) under a specific condition. In another study, *Martin et al. (2017)* applied GBM to assess the topological similarity between networks (from *E. coli*) under different biological conditions. Previous research on network analyses focused on graphlets composed of three nodes only; however, the extension of graphlets with four nodes is still limited (*Trpevski et al., 2016*; *Martin et al., 2016*; *Martin et al., 2017*).

Furthermore, *Zenil, Kiani & Tegnér (2013)* applied the Block Decomposition Method to estimate algorithmic probability of the four-node motifs of a network, the authors demonstrated that their method correctly distinguish the developmental genetic network and the signal transduction network, the performance is better than the compression algorithm, BZIP2.

Many tools (*Tran et al., 2015*; *Meira et al., 2018*; *Meira et al., 2014*; *Wernicke & Rasche, 2006*; *Omidi, Schreiber & Masoudi-Nejad, 2009*; *Meira et al., 2014*) have been developed to detect 'statistically significant' network motifs. The *acc-Motif* algorithm can identify network motifs with a size of up to five nodes. Later, the algorithm was improved to find motifs for up to six nodes (*Meira et al., 2018*). We noted that the tool *LoTo* identifies motifs for up to three nodes but not for four nodes. But these tools may not be able to detect the complete set of motifs, because the predicted patterns are not statistically significant. This suggests that motif-finding tools have limitations in our earlier work (*Huang et al., 2020*), as they cannot enumerate all the network motifs embedded in a network due to the use of an arbitrary threshold; *i.e.*, p-value is larger than 0.05. Also, it is known that the time complexity of identifying N-node motifs in a large network is an NP-complete problem (*Kim et al., 2013*).

The network subgraph-based approach and network comparison

Mowshowitz (1968), who developed a method to address the problem of gauging the relative complexity of graphs. Drawing on that, in our previous work (*Huang et al., 2020*) we propose the network subgraph-based approach, treat the network subgraphs' pattern *exactly* the same as the network motifs. but not make use of the randomization definition to extract the subgraphs embedded in a network.

Network similarity can be quantified by using the information-theoretic quantity Kullback–Leibler entropy (H_{KL}). In 2011, *Kugler et al. (2011)* introduced the use of graph prototyping for network comparison. They showed that in three out of the five graph distance measures used, the group of prostate cancer networks differed significantly from the group of benign networks. H_{KL} is an asymmetric quantity, one can define a symmetric quantity, H_{JS}, to gauge network similarity.

Our method is an alignment-free approach. It is different from some earlier studies (*Sarajlić et al., 2016*; *Trpevski et al., 2016*; *Martin et al., 2016*; *Martin et al., 2017*) in that we employed a subgraph instead of a graphlet to dissect network topologies.

In the 'Methods' section, we present our approach, introduce network comparison method and describe setting up simulation experiments to test our method. In the 'Results' section, we present the effectiveness of our approach on simulated data, and its use to evaluate similarities amongst three categories of molecular biology networks. We also address the biological meanings of topological similar molecular networks. In the 'Conclusion' section, we elaborate the key findings in this work, and suggest biological applications of our method in future study.

METHODS

Network subgraph-based approach

Mowshowitz (1968) proposed that a finite graph (N nodes and E edges) can be decomposed into equivalence classes (C classes); each class contains n_i nodes, and a probability is assigned to each class, *i.e.*, $p_j = n_j/N$. There are many ways of partitioning the set of nodes of a graph, one way to obtain a decomposition is to identify the orbits of a graph. The orbits of a graph can be identified by calculating the degree of the nodes, point-deleted neighborhood degree vector and betweenness centrality (*Mowshowitz & Mitsou, 2009*). The subgraph-based approach we developed does not rely on determining the orbits of a graph; hence, it is a different one.

Adjacency matrix

Given a network subgraph, one can construct an adjacency matrix A, with matrix elements "0" and "1" to represent the absence and presence of connections among the nodes, respectively. Each subgraph can be represented by a decimal. This can be achieved by arranging all the entries in the adjacency matrix by row major order into one binary string and then convert it to decimal, each subgraph can be denoted by an unique decimal value, called graph ID.

Subgraph identification, network comparison and simulation experiments

Previously, we developed a subgraph detection algorithm, *PatternFinder* (*Huang et al., 2020*), to identify three-node subgraphs and four-node subgraphs embedded in cancer networks, STN, and cellular processes. A brief description of the algorithm, *PatternFinder,* was provided in the Appendix section. Also, we point out that *PatternFinder* is an exhaustive search algorithm, which allowed us to detect the complete set of subgraphs and subgraphs within a subgraph, it is not intend for large-scale network analysis.

In information theory, a number of quantities can be used to characterize the distance between two probability distributions. For instance, one can use the Kullback–Leibler entropy, H_{KL}, also known as cross-entropy (*Capra & Singh, 2007*) to quantify the distance. Given two discrete probability distributions, X and Y, the Kullback–Leibler entropy of X with respect to Y is defined by

$$H_{KL}(X||Y) = -\sum_i X_i \log \frac{X_i}{Y_i}. \quad (1)$$

H_{KL} is asymmetric under the interchange of X and Y. In 2011, *Kugler et al. (2011)* introduced the use of H_{KL} for network comparison. They showed that in three out of the five graph distance measures used, the group of prostate cancer networks differed significantly from the group of benign networks.

One can symmetrize H_{KL} by adding the term $H_{KL}(Y||X)$. We applied a similar quantity, H_{JS}, to gauge network similarity. H_{JS} is a symmetric function and is used to measure the distance between the two subgraph probability distributions X and Y for networks N_X and N_Y, respectively. H_{JS} is defined as follows:

$$\boldsymbol{H_{JS} = \frac{1}{2}[H_{KL}(X||Z) + H_{KL}(Y||Z)]}. \quad (2)$$

where $Z = \frac{1}{2}(X + Y)$.

Let $X^{(n)}$ and $Y^{(n)}$ be the n-node subgraph probability distributions obtained by using *PatternFinder* for networks N_X and N_Y, respectively, where $n = 3$ or 4. If n equals to 3, $X^{(3)}$ and $Y^{(3)}$ are compose of thirteen components; obviously, $X^{(4)}$ and $Y^{(4)}$ are compose of 199 components. Then, the three-node subgraph Jensen–Shannon entropy measure for networks N_X and N_Y , $H_{JS}^{(3)}$ is given by

$$H_{JS}^{(3)} = \frac{1}{2}\left[\boldsymbol{H_{KL}}\left(\boldsymbol{X}^{(3)}||\boldsymbol{Z}^{(3)}\right) + \boldsymbol{H_{KL}}\left(\boldsymbol{Y}^{(3)}||\boldsymbol{Z}^{(3)}\right)\right] \quad (3)$$

where $Z^{(n)} = \frac{1}{2}(X^{(n)} + Y^{(n)})$, with $n = 3$. A similar expression for the four-node subgraph Jensen–Shannon entropy measure, $H_{JS}^{(4)}$, can be obtained simply by substituting $X^{(4)}$, $Y^{(4)}$ and $Z^{(4)}$ into Eq. (3).

The unique feature of H_{JS} is that it measures the similarity between two networks in terms of the underlying architecture of the networks rather than the identities of the nodes. In other words, network similarity is measured without referring to the genetic identities of a subgraph. The square root of H_{JS} is a metric called the Jensen–Shannon distance (*Endres & Schindelin, 2003*).

H_{JS} has been used in many applications, such as (i) predicting functionally important amino acids from sequence conservation, (ii) pattern recognition in bioinformatics (*Loog et al., 2011*), (iii) predicting important non-conserved residues in protein sequences (*Gültas et al., 2014*), (iv) analyzing DNA sequences (*Grosse et al., 2002*), and (v) measuring the distance between random graphs (*Wong & You, 1985*). *Wong & You (1985)* proposed a distance metric between two random graphs based on the smallest change in Shannon entropy before and after merging the two random graphs.

In order to verify the effectiveness of the subgraph-based approach along with the H_{JS} metric, we used the 'igraph' package (*Csardi & Nepusz, 2006*) (https://igraph.org/) to

Table 1 Description of the six network models, 'igraph' parameter settings and meaning of the parameters.

Network type	Description of the network (igraph)	parameters used in 'igraph'
Random graph	This model is very simple, every possible edge is created with the same constant probability	Prob = 0.0188, directed = TRUE
Scale-free network	The BA-model is a very simple stochastic algorithm for building a graph	Power = 2, m = 3, zero.appeal = 1, directed=TRUE, algorithm=psumtree
Small world	Generate a graph according to the Watts–Strogatz network model	Dim = 1, Nei = 25, p = 0.6, directed = TRUE
Geometric random graph	Generate a random graph based on the distance of random point on a unit square	radius = 0.15, torus = TRUE, coords = TRUE, directed = TRUE
Aging random graph	This function creates a random graph by simulating its evolution. Each time a new vertex is added it creates a number of links to old vertices and the probability that an old vertex is cited depends on its in-degree (preferential attachment) and age	pa.exp = 1, aging.exp = −1, aging.bin = 1,000, directed = TRUE
Citation random graph	creates a graph, where vertices age, and gain new connections based on how long ago their last citation happened	edges = 1, age_bins=nodes/100 agebins,pref = (1:(agebins + 1)) 3, directed = TRUE

generate six different network models (Random graph, Scale-free network, Small world, Geometric random graph, Aging random graph, Citation random graph, using three different number of nodes: 300, 400 and 500, and two types of edge density: 2% and 6%, each network repeated three times, *i.e.*, a total of 6*3*2*3 = 108 networks) and then used MST-kNN (*Arefin et al., 2014*) to perform clustering classification. MST-kNN is an unsupervised graph-based clustering classifier based on Jensen–Shannon divergence and graph partition algorithm, it was utilized to classify the authorship of drama and poems. Table 1 described these six models, 'igraph' parameter settings (*Csardi & Nepusz, 2006*), and meaning of the parameters.

Input datasets—cancer networks, signal transduction networks (STN) and cellular processes

Network information was retrieved from the KEGG database (*Nakaya et al., 2013*). After manual inspection, we removed networks composed of separate components, such as "chemical carcinogenesis", "microRNAs in cancer", "two-component system", and "viral carcinogenesis". In addition, we collected the networks labelled with "signaling pathway", grouped them together, and called them "signal transduction networks (STN)". We note that STN range across different families of molecular networks recorded by KEGG, including "endocrine system", "immune system", and "signal transduction". We compiled three major types of molecular networks, *i.e.*, 17 cancer networks, 45 STN, and nine cellular processes. Names of these three types of molecular networks are listed in File S1.

Table 2 Summary of the parameters of three simulation experiments, including six network models, network sizes, edge densities, total number of networks, and classification accuracy.

simulation	Network type	Network sizes	Edge density	Total number of networks	Accuracy
I	Random graph, Scale-free network, Small world, Geometric random graph, Aging random graph, Citation random graph	300, 400, 500	2%	54	100%
II	Random graph, Scale-free network, Small world, Geometric random graph, Aging random graph, Citation random graph	300, 400, 500	6%	54	100%
III	Small world, Aging random graph, Citation random graph	300, 400, 500	2% & 6%	54	100%

We downloaded the KGML files of the 71 networks from the KEGG database and used the Cytoscape plug-in tools KEGGScape (*Nishida et al., 2014*) and KEGGparser (*Arakelyan & Nersisyan, 2013*) to obtain node and edge information for those networks. Real-world molecular networks are composed of thousands of genes, which are larger than the networks we analyzed; however, the regulatory and feedback interaction information among thousands of genes are not available in KEGG, yet it can be analyzed once the data are available.

RESULTS

Comparison of tools—*PatternFinder*, *acc-Motif* and *LoTo*

To evaluate the performance of *PatternFinder* in enumerating all the three-node subgraphs, we have demonstrated the usefulness of tool in Table 2 of our previous study (*Huang et al., 2020*).

Essentaily speaking, *PatternFinder* is able to identify the complete set of subgraphs, whereas *acc-Motif* identifies relatively few network motifs. Furthermore, *acc-Motif* is unable to identify some of the four-node subgraphs for a given network due to the fact that those subgraphs are not statistically significant. Also, we noted that the tool *LoTo* identifies motifs for up to three nodes but not for four nodes. The above results suggest that motif-finding tools may have certain limitations as they cannot enumerate all possible substructures of a network. We provided Files S2 and S3 to help the reader relate (i) the subgraphs' decimals and their graphical representation, and (ii) the *acc-Motif* IDs and their graphical representation.

Given the three-node subgraphs and four-node subgraphs identified by *PatternFinder*, the normalized frequency distributions of the thirteen three-node subgraphs and 199 four-node subgraphs were determined; hence, network similarity was quantified by using the information-theoretic quantity H_{JS}.

Classification of network models using subgraph-based approach

To examine the effectiveness of the subgraph-based approach, we applied the method along with H_{JS} to classify six network models. We considered three types of simulations (Table 2). Simulations I and II consider six network models, each model with three different node numbers, but with the same edge density, *i.e.*, 2% and 6% respectively; and repeat the

simulation for three trials, therefore, each simulation composes of $6 \times 3 \times 3 = 54$ networks need to classify. The third simulation considered three network models; with different numbers of nodes and edge densities, again there are 54 networks ($3 * 3 * 2 * 3 = 54$) to classify.

Given the 54 networks, we performed the following: (i) applied *PatterFinder* to extract the three-node subgraph probability distribution for each network, (ii) computed the pairwise H_{JS} distance matrix (a matrix with dimension 54×54, File S4 summarizes the H_{JS} values for the three simulations), and (iii) used the MST-kNN package to do cluster analysis. The results of classification achieve 100% accuracy for the three simulations (Table 2 last column & Figs. 1A–1C). For example, Fig. 1A shown that the 54 networks are correctly classified into six network models. Orange color circles in Fig. 1A denote "Geometric Random Graph", the numbers listed inside the circles start from 1 to 9, which are the first nine networks in the pairwise H_{JS} distance matrix. Similarly, the blue colored circles included numbers run from 10 to 18, which represent "Random Graph". We checked the numbers listed in the other four different colored circles, which correctly denote the other four types of network models. The result of Fig. 1C shows that given the H_{JS} distance matrix, the MST-kNN classifier correctly classify the six possibilities (three network models along with two different edge densities). Compared with the results presented in *Sarajlić et al. (2016)*, our classification accuracy is better; but the network we analyzed is relatively small, the number of nodes is not more than 500.

File S5 provided the codes for (i) generating the six models, (ii) calculating the H_{JS}, and (iii) performing cluster analysis using MST-kNN.

To address the concern why our method can distinguish networks with similar global topology, we provide a detail discussion in File S6. In essence, we plot the cumulative probability functions ('cpfs') of the three-node subgraphs for the first trial; so there are 18 'cpfs'. As shown in the Fig. S6.1, the small-world and scale-free networks 'cpfs' can be clearly distinguished from the rest. Among the other four random networks, the 'cpfs' of aging random network and citation random network are quite close but with minor difference, as shown in Fig. S6.2; thus, indicates the effectiveness of our method.

Cancer networks

We performed a pairwise network comparison between the 17 cancer networks, computed the H_{JS} distances, and ranked the H_{JS} distances from the smallest to the largest. Table 3 lists the results for the top three most similar pairs of cancer networks based on the H_{JS} distance. It is noted that the H_{JS} distance is non-zero, and the value may be as small as 0.0214. In other words, no two networks have exactly the same subgraph frequency distributions. The complete list of the H_{JS} distances of the cancer networks is given in File S7.

The degree of similarity between two networks is characterized by subgraph frequency distributions. Given a pair of highly similar networks, we calculated the absolute values of the difference of the normalized frequency distributions of the network subgraphs. The magnitude of the difference (both three-node and four-node subgraphs) can be seen in the right-hand side of Table 3. The range of difference of the three-node subgraph distributions for the "acute myeloid leukemia (AML)" network and the "pancreatic cancer" network is

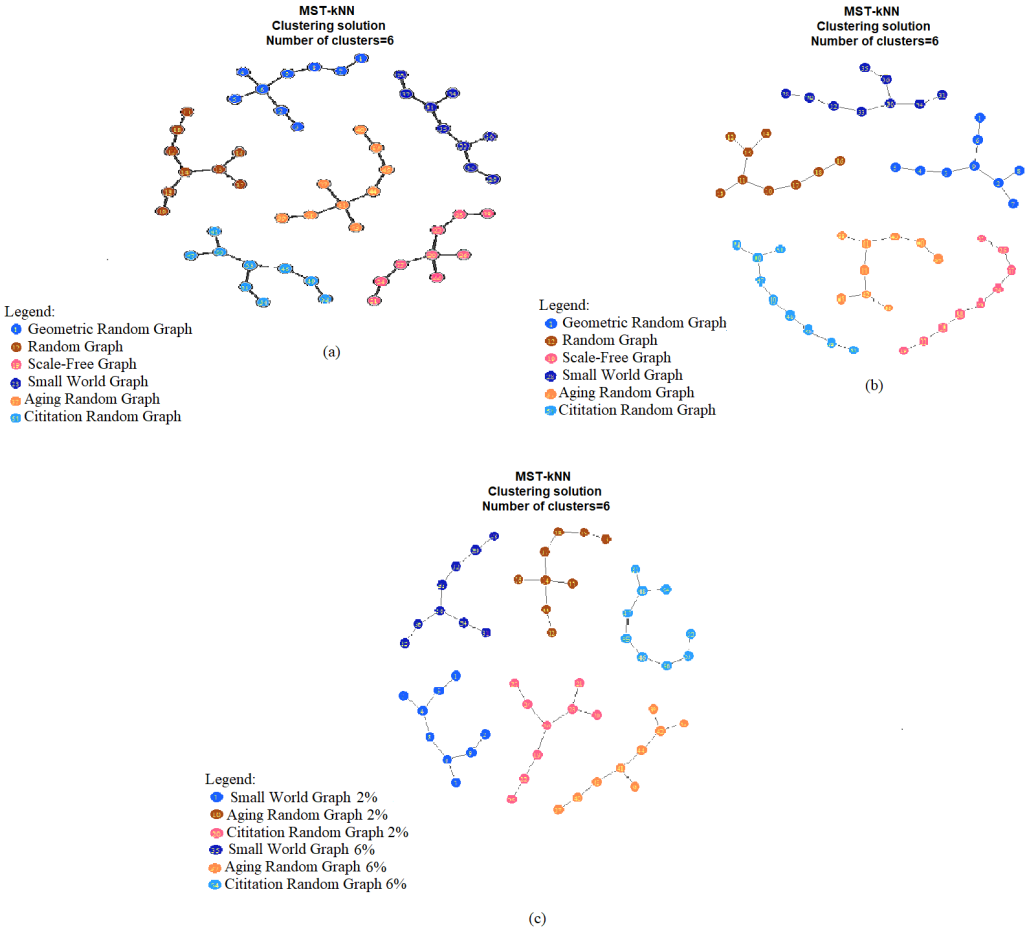

Figure 1 **Visualization of the results of classification for (A) simulation I, (B) simulation II and (C) simulation III, using MST-kNN.**

Full-size DOI: 10.7717/peerj.13137/fig-1

Table 3 **The top three most similar pairs of cancer networks based on the H_{JS} distance of the three-node subgraphs and four-node subgraphs normalized frequency distributions.**

Network A	Network B	H_{JS} distance	Absolute value of the difference of the subgraph normalized frequency distributions
3-node subgraph ID			(ID 6, ID 12, ID 36, ID 38)
Acute myeloid leukaemia (AML)	Pancreatic cancer	0.0214	(0.013, 0.007, 0.021, 0.002)
Chronic myeloid leukaemia (CML)	Gastric cancer	0.0309	(0.038, 0.020, 0.018, null)
Gastric cancer	Small cell lung cancer	0.0339	(0.024, 0.042, null, 0.018)
4-node subgraph ID			(ID 14, ID 28, ID 74, ID 76, ID 78, ID 280, ID 328, ID 392, ID 2184)
Gastric cancer	Hepatocellular carcinoma	0.0998	(0.001, 0.027, 0.063, 0.011, null, 0.001, 0.045, 0.046, 0.006)
Chronic myeloid leukaemia (CML)	Melanoma	0.138	(0.009, 0.049, 0.114, 0.017, null, 0.028, 0.016, 0.016, null)
Hepatocellular carcinoma	Small cell lung cancer	0.138	(0.115, 0.006, 0.025, 0.015, null, 0.004, 0.004, 0.065, 0.002)

0.002–0.021, which is smaller than the ranges for the other two pairs of cancer networks. Both the "AML" and "pancreatic cancer" networks are characterized by the frequency distributions of four subgraphs: SIM (id_6), cascade (id_12), MIM (id_36), and FFL (id_38). The word "null" denotes that the subgraph normalized frequency distribution is zero. In our previous study (*Huang et al., 2020*), we have shown that subgraphs "id_6", "id_12", and "id_36" are not composed of any three-node subgraphs. We considered that these three subgraphs exhibit the property of *irreducibility* (a N-node subgraph does not embed any other N-node subgraph) (*Huang et al., 2020*).

The range of difference of the four-node subgraph distributions for "gastric cancer" and "hepatocellular carcinoma" is 0.001–0.0046, which is lower than those of the other two pairs of cancer networks.

We formally define the *irreducibility* property of a graph as follows: for the set of N-node directed graph, graph G is said to be irreducible if graph G has exactly N-1 links. It is easy to see that the graph with irreducibility property is the basic block for constructing the N-node structure motifs. For the four-node subgraphs: "id_14" (SIM), "id_28", "id_74", "id_76" (MIM), "id_280", "id_328" (cascade), "id_392", and "id_2184", we considered these eight subgraphs also exhibit the property of irreducibility (*Huang et al., 2020*). In fact, we found that the underlying substructures of molecular networks are dominated by irreducible subgraphs, and accordingly, this behavior also holds true for the STN and cellular process networks. According to our previous work (*Huang et al., 2020*), the 'reciprocity' of these 'irreducible building blocks' are all negative. Reciprocity is a parameter that quantifies the degree of bidirectional connection of a network subgraph. Molecular networks are mostly composed of these types of subgraphs, a possible reason is that the signal can be quickly transmitted from the cell membrane to the nucleus, there is no feedback signal. Furthermore, since the irreducible subgraphs are the dominate subgraphs of molecular networks, one can apply the dimension reduction technique to reduce the complexity of large networks, while preserving the algorithmic information content the networks very well (*Zenil, Kiani & Tegnér, 2015*; *Kiani et al., 2016*).

Given the three-node subgraph normalized frequency distributions of the 17 cancer networks, the AML and pancreatic cancer networks (hsa05221 and hsa05212) exhibited the smallest H_{JS} distance. We used the "User data mapping" application provided by the KEGG resource, and accordingly, the regulatory relations among the genes embedded in the three-node subgraph module (blue color) are depicted in Figs. 2A and 2B. According to the KEGG annotation, both networks involve six common biological processes. These six processes are located in three different regions in Figs. 2A and 2B. The upper part of Figs. 2A and 2B refers to the PI3K-Akt, MAPK, and Jak-STAT signaling processes; the right-hand part consists of the apoptosis and proliferation process; and the lower part includes the cell cycle process. Thus, our findings suggest that the underlying signaling mechanisms and cellular processes associated with the two networks are highly similar. These results are unexpected because the identities of the genetic elements are not considered in our calculations, and the results are inferred only from the subgraph frequency distributions. This study takes an important step in the direction of defining the relationship between subgraph distributions and subgraph-associated signal transduction and/or cellular processes. For instance, for

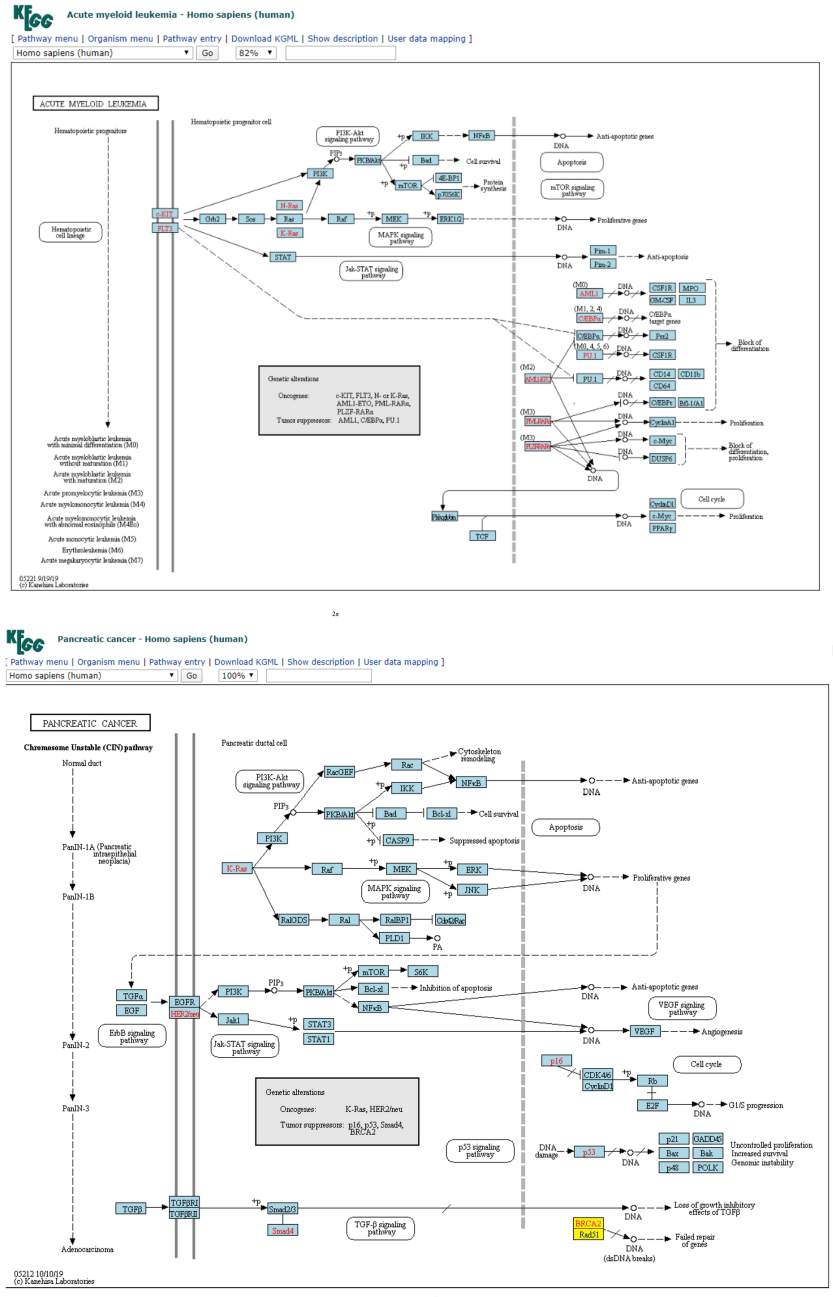

Figure 2 **(A) Three-node subgraph module of the AML network. (B) Three-node subgraph module of the pancreatic cancer network.** Blue color boxes denote genes embedded in a subgraph module. Other colored objects denote genes which are not belong to a subgraph module, red color fonts mean genetic alternation (oncogene or tumor suppressor gene).

Full-size DOI: 10.7717/peerj.13137/fig-2

both AML and pancreatic cancer, the Ras-PI3K-PKB/Akt subgraph and Ras-Raf-MEK subgraph are associated with the PI3K-Akt and MAPK signal transduction pathways, respectively.

Furthermore, similar observations were found when considering four-node subgraph frequency distributions. Genes embedded in the four-node subgraph modules of the gastric cancer and hepatocellular carcinoma networks are depicted in Figs. 3A and 3B, respectively. Genes embedded in the four-node subgraph modules are shown in blue. It is clear that both cancer networks are mainly composed of the "SIM" pattern (id_14) and the "id_280" pattern (id_280). As shown in Table 3, the H_{JS} distance of id_6 is as small as 0.001. According to the annotation provided by KEGG, both cancer networks involve six common processes. The left-hand part consists of the Wnt, PI3K-Akt, TGF-β, and MAPK signaling processes, and the right-hand part consists of the cell cycle and proliferation processes.

For four-node subgraphs, the above figures shown that we have identified the scaffold (the annotation provided by KEGG), it is a set of physically bound proteins which maintain the specificity of the signal transduction pathway and catalyze the activation of the pathway components (*Burack & Shaw, 2000*). In a review article, Koch reported out that the forkhead box family transcription factors may affect the Wnt signaling activity that leads to various types of cancer (*Koch, 2021*), and Wnt pathway is a drug therapeutic target (*Krishnamurthy & Kurzrock, 2018*; *Jung & Park, 2020*). The above findings provide an example of biological application of our approach.

In Fig. 4A, we plotted the normalized frequency of the three-node subgraphs for the three pairs of cancer networks. The AML network and the "pancreatic cancer" network were found to be highly similar because the H_{JS} distance is the smallest among all possible pairwise comparisons. Figure 4A depicts that the red and green dots are located close to each other for the following four subgraphs: SIM (id_6), cascade (id_12), MIM (id_36), and FFL (id_38); hence, the H_{JS} distance between the AML and pancreatic cancer networks is minimal.

"Chronic myeloid leukemia (CML)" and "gastric cancer" are associated with the second smallest H_{JS} distance. These two networks are characterized by similar frequency distributions of the following subgraphs: SIM, cascade, and MIM (Fig. 4A, purple and blue dots).

Biological interpretation—cancer networks

Regarding the practicality of our approach, we show that our method is able to cluster cancer networks with similar underlying regulatory topology. It was found that the AML and pancreatic cancer networks exhibited the smallest H_{JS} distance. AML and pancreatic disease have been reported to be observed simultaneously in some patients during clinical diagnosis (*Cascetta et al., 2014*). Pancreatic masses develop during or after AML (*Messager et al., 2012*). AML can rarely mimic the clinical picture of pancreatic cancer (*Schafer et al., 2008*), while pancreatitis is a characteristic in the appearance of AML (*De Castro, Vencer & Espinosa, 2017*). According to the KEGG annotation, both cancer networks involve three common signaling pathways; that is. PI3K-Akt, MAPK and Jak-SAT. For instance, given

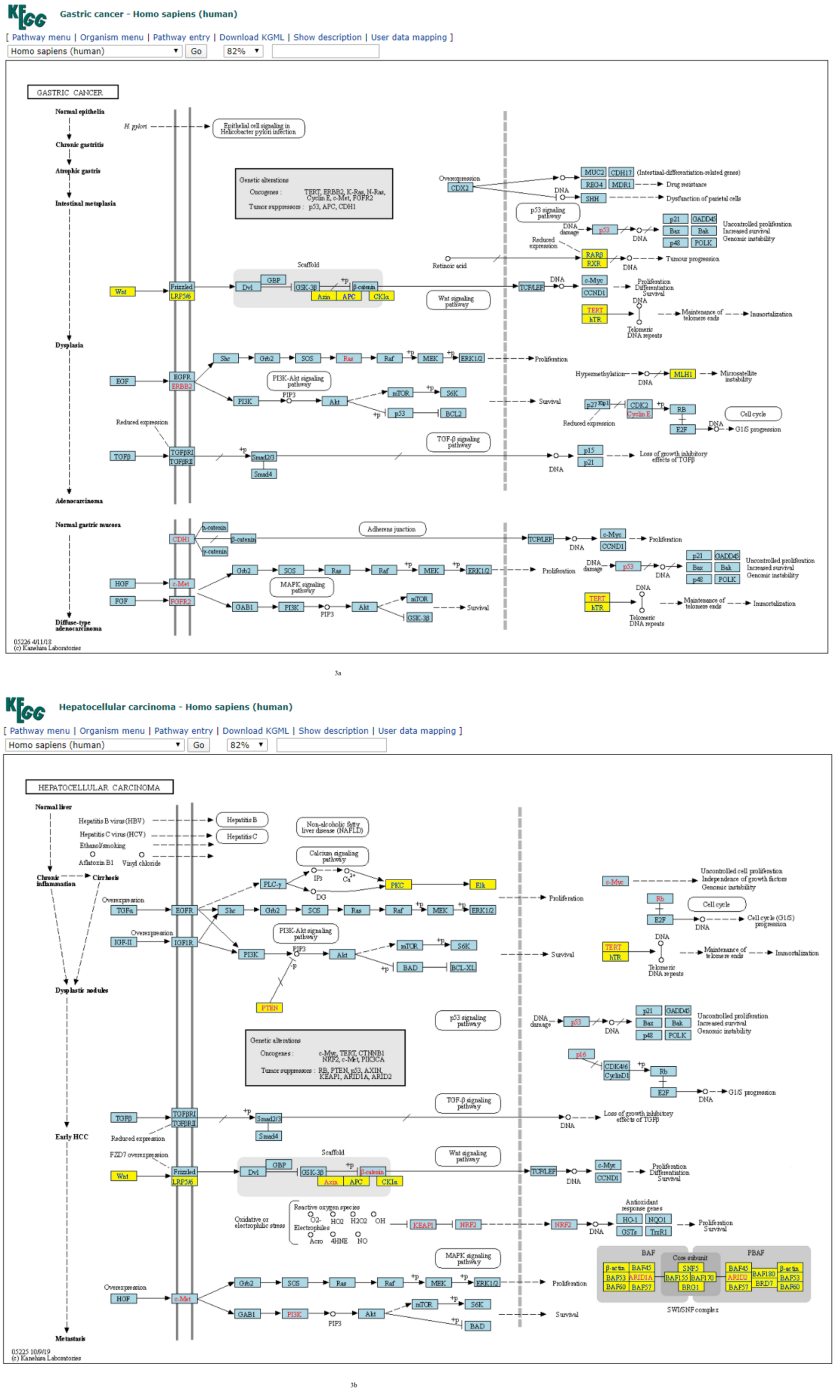

3a

3b

Figure 3 **(A) Four-node subgraph module of the gastric cancer network. (B) Four-node subgraph module of the hepatocellular carcinoma network.** Blue color boxes denote genes embedded in a subgraph module. Other colored objects denote genes which are not belong to a subgraph module, red color labels mean genetic alternation (oncogene or tumor suppressor gene), and grey colored rectangle in the middle of Figs. 3A and 3B denote scaffold (KEGG annotation).

Full-size DOI: 10.7717/peerj.13137/fig-3

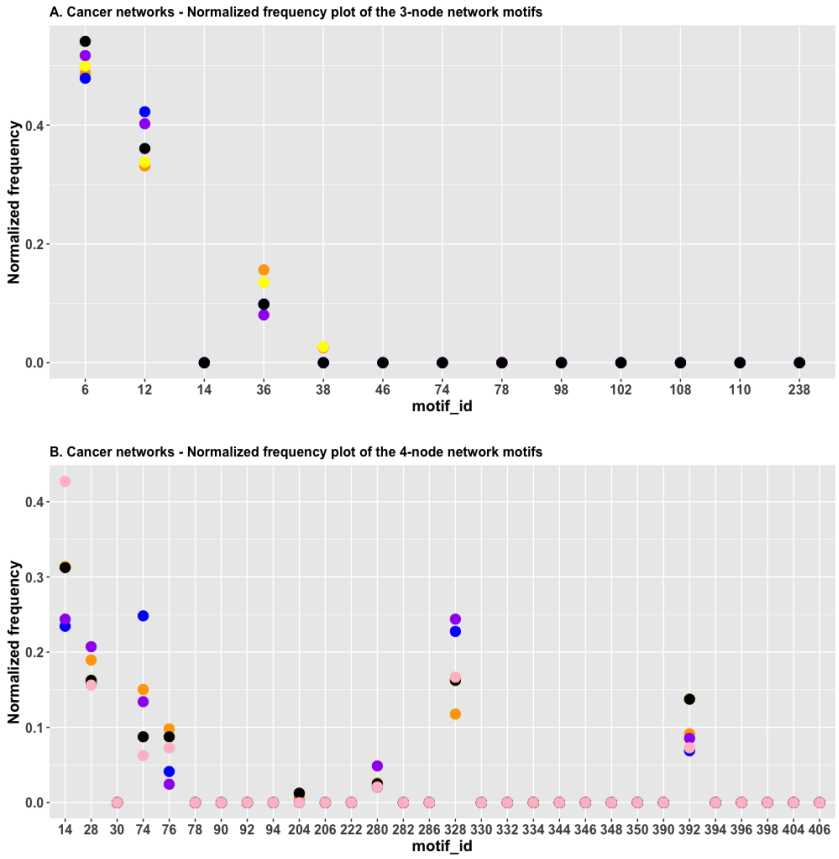

Figure 4 **(A) The plot of the normalized frequency of the three-node subgraphs for the three pairs of cancer networks with the smallest H_{IS} distance. Color labelling of the cancer types: AML (orange), pancreatic cancer (yellow), CML (blue), gastric cancer (purple) and small cell lung cancer (black). (B) The plot of the normalized frequency of the four-node subgraphs for the three pairs of cancer networks with the smallest H_{IS} distance. Color labelling of the cancer types: Gastric cancer (orange), Hepatocellular carcinoma (yellow), Chronic myeloid leukaemia (blue), Melanoma (purple) and Small cell lung cancer (black).**

Full-size DOI: 10.7717/peerj.13137/fig-4

the common PI3K-Akt pathway found in both diseases, we found the following two sets of common activation relationships: (i) Ras → PI3K → PKB/Akt → IKK → NFkB, and (ii) Ras → raf → MEK → ERK. Thus, the results suggest that the underlying signaling mechanisms associated with the two cancer diseases are highly similar. Even though some of the genes are different in the two diseases, the same signaling mechanisms are involved; hence, the subgraph-based approach take us from the subgraph level to the mechanism level interpretation.

For the second pair of networks, previous studies have shown that (i) both CML and gastric cancer might co-exist in a single patient (*Butala, Kalra & Rosner, 1989*), which might be due to decreased immunity (*Mangal et al., 2018*), and (ii) clinicians are recommended to pay attention to the association of CML and gastric cancer (*Mokhtarifard et al., 2016*) and expression of *MMP1* may contribute to gastric cancer formation (*Yang et al., 2017*).

For the third pair of networks, it has been reported that (i) gastrointestinal metastases from lung cancer are diagnosed at a late stage and are thus life-threatening (*Li et al., 2018*); (ii) gastric cancer metastasis may result from lung cancer (*Gao et al., 2015*); (iii) gastric cancer is associated with lung cancer (*Park, 1998*; *Snyder et al., 2013*; *Nitipir et al., 2018*; *Koh & Lee, 2014*) ; (iv) both diseases can be successfully treated with carboplatin (*Sano et al., 1986*). The use of natural products along with chemotherapy drugs are effective in treating lung cancer (*Huang et al., 2017*).

Figure 4B depicts the plot of the normalized frequency distributions of the four-node subgraphs for cancer networks. The normalized frequency counts of most of the four-node subgraph patterns are zero; therefore, only the IDs of the first 30 subgraphs (sorted according to the decimal representation) are shown. The difference between the distributions in gastric cancer (red) and hepatocellular carcinoma (HCC) (green) is minimal among the following subgraphs: id_14, id_28, id_76, id_204, and id_280, whereas the difference between CML (blue) and melanoma (purple) is minimal among a different set of subgraphs: id_14, id_76, id_204, and id_328.

According to many studies, (i) both gastric cancer and HCC can co-exist in the same patient (*Sakumura, Tajiri & Sugiyama, 2018*; *Hu et al., 2014*); (ii) optimal surgical strategies have been developed for treating synchronous gastric cancer and HCC (*Tawada et al., 2014*; *Uenishi et al., 2003*); and (iii) it is necessary to closely follow up patients with gastric cancer or HCC for an early diagnosis (*Chen et al., 2017*). Next, we used the *R* package to perform cluster analysis of the cancer networks based on the H_{JS} distance measure. In Figs. 5A and 5B, we show the heatmap of the cancer networks using the H_{JS} distance of the three-node subgraphs and the four-subgraph nodes, respectively. For the three-node subgraphs, we identified the following three pairs of highly similar networks: (i) ‘‘acute myeloid leukemia’’ and ‘‘pancreatic cancer’’, (ii) ‘‘gastric cancer’’ and ‘‘small cell lung cancer’’, and (iii) ‘‘chronic myeloid leukemia’’ and ‘‘hepatocellular carcinoma’’. For the four-node subgraph clustering results, the following highly similar pairs are detected: (i) ‘‘gastric cancer’’ and ‘‘hepatocellular carcinoma’’, (ii) ‘‘chronic myeloid leukemia’’ and ‘‘melanoma’’, and (iii) ‘‘basal cell carcinoma’’ and ‘‘small cell lung cancer’’. In the majority, the results of the identified pairs of networks are consistent with the findings listed in Table 3.

From Fig. 5A, we noted two regions associated with a similar color, *i.e.*, the upper left-hand and lower right-hand corners. Similar patterns can be found for the four-node subgraphs, *i.e.*, Fig. 5B. The result suggests a group of cancer networks possess similar subgraph topology.

Signal transduction network (STN)

A list of the top three most similar STN is given in Table 4. The range of difference for the three-node subgraph distributions of the first pair of highly similar networks, ‘‘sphingolipid signaling pathway’’ and ‘‘TGF-beta signaling pathway’’, is 0.001–0.029, which is relatively small when compared to the other two pairs of pathways. The range of difference for the four-node subgraph distributions of the first pair of highly similar networks is 0.001–0.034, which is lower than that of the other two pairs of the STN. Again, it was found that the

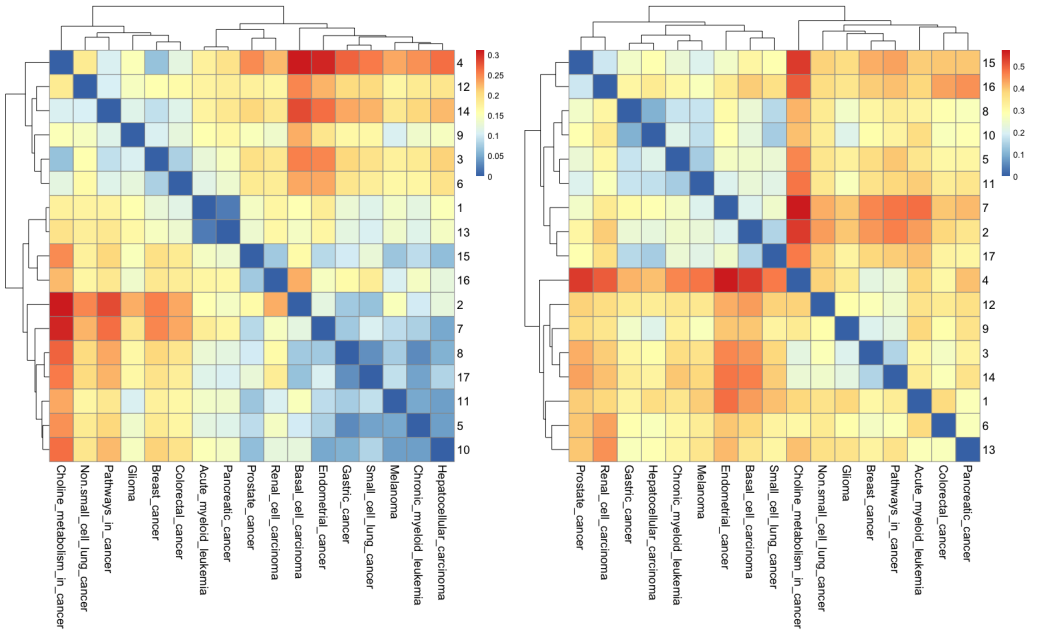

Figure 5 The heatmap of H_{js} distance computed for cancer networks: (A) three-node subgraphs and (B) four-node subgraphs, with light yellow and darker red denote the small and large value of H_{js} respectively. The number of each row denotes the network name (File S1).

Full-size DOI: 10.7717/peerj.13137/fig-5

Table 4 The top three most similar pairs of STN based on the H_{JS} distance of the three-node subgraphs and four-node subgraphs normalized frequency distributions.

Network A	Network B	H_{JS} distance	Absolute value of the difference of the subgraph normalized frequency distributions
3-node subgraph ID			(ID 6, ID 12, ID 36, ID 38)
Sphingolipid signaling pathway	TGF-beta signaling pathway	0.0263	(0.001, 0.029, 0.026, 0.005)
ErbB signaling pathway	Hippo signaling pathway	0.0312	(0.015, 0.017, 0.037, 0.005)
PI3K-Akt signaling pathway	Ras signaling pathway	0.0330	(0.010, 0.010, 0.007, 0.007)
4-node subgraph ID			(ID 14, ID 28, ID 74, ID 76, ID 78, ID 280, ID 328, ID 392, ID 2184)
Neurotrophin signaling pathway	Ras signaling pathway	0.115	(0.034, 0.030, 0.033, 0.026, 0.018, 0.024, 0.019, 0.008, 0.001)
Adipocytokine signaling pathway	B-cell receptor signaling pathway	0.119	(0.017, 0.054, 0.035, 0.034, 0.001, 0.013, 0.012, 0.031, 0.007)
Apelin signaling pathway	Chemokine signaling pathway	0.131	(0.045, 0.037, 0.011, 0.016, 0.005, 0.029, 0.010, 0.016, 0.007)

underlying substructure of the molecular networks is dominated by irreducible subgraphs. The complete list of the H_{JS} distances of the STN is given in File S7.

Figure 6A depicts the normalized frequency distributions of the three-node subgraphs for STN. Figure clearly shows that the red and green dots are located close to each other for the following four subgraphs: id_6, id_12, id_36, and id_38. This indicates that the H_{JS} distance between the "sphingolipid signaling pathway" and "TGF-beta signaling pathway"

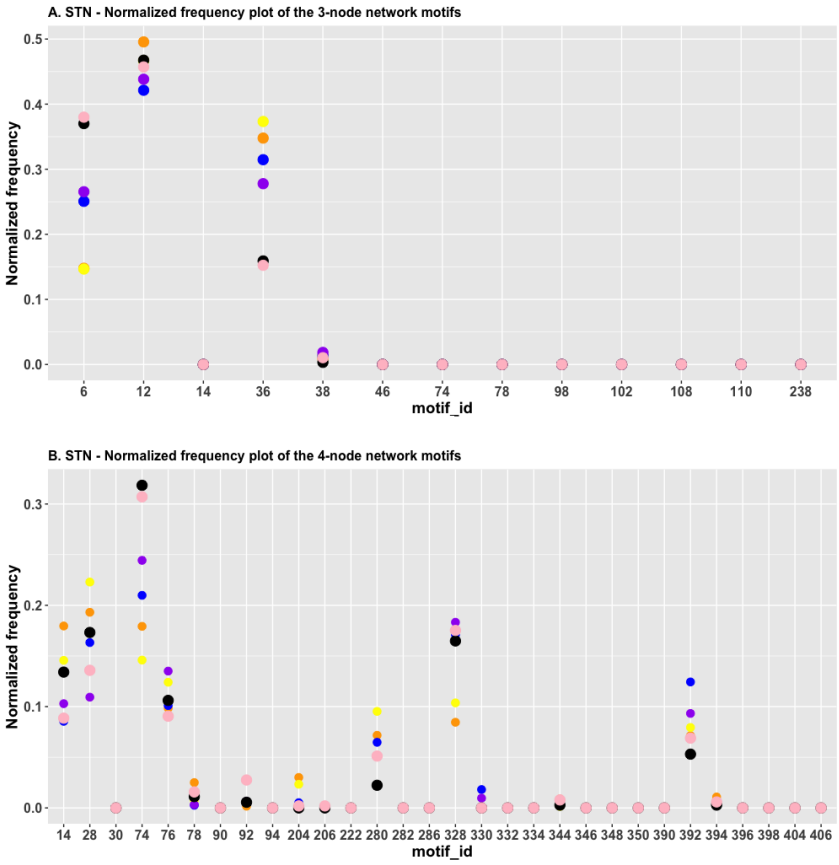

Figure 6 **(A) The plot of the normalized frequency of the three-node subgraphs for three pairs of STN with the smallest H_{JS} distance.** Color labelling of the STN is: Sphingolipid signaling pathway (orange), TGF-beta signaling pathway (yellow), ErbB signaling pathway (blue), Hippo signaling pathway (purple), PI3K-Akt signaling pathway (black) and Ras signaling pathway (pink). (B) The plot of the normalized frequency of the four-node subgraphs for the three pairs of STN with the smallest H_{JS} distance. Color labelling of the STN are: Sphingolipid signaling pathway (orange), Ras signaling pathway (yellow), Adipocytokine signaling pathway (blue), B-cell receptor signaling pathway (purple), Apelin signaling pathway black) and Chemokine signaling pathway (pink).

Full-size DOI: 10.7717/peerj.13137/fig-6

is minimal. The blue and purple dots are located close to each other for the same set of subgraphs, suggesting that the H_{JS} distance between the "ErbB signaling pathway" and the "Hippo signaling pathway" is minimal. Similarly, the black and pink dots are located close to each other, implying a low H_{JS} distance between the "Apelin signaling pathway" and the "chemokine signaling pathway".

Biological interpretation—STN

For the STN three-node subgraph case, the most similar pair of networks is the "sphingolipid signaling pathway" and the "TGF-beta signaling pathway". *Dennler, Goumans & Ten Dijke (2002)* demonstrated that endogenous sphingolipid mediators are involved in regulating the TGF-beta signaling pathway. This is further supported by two other studies, which demonstrated cooperation between TGF-beta and S1P

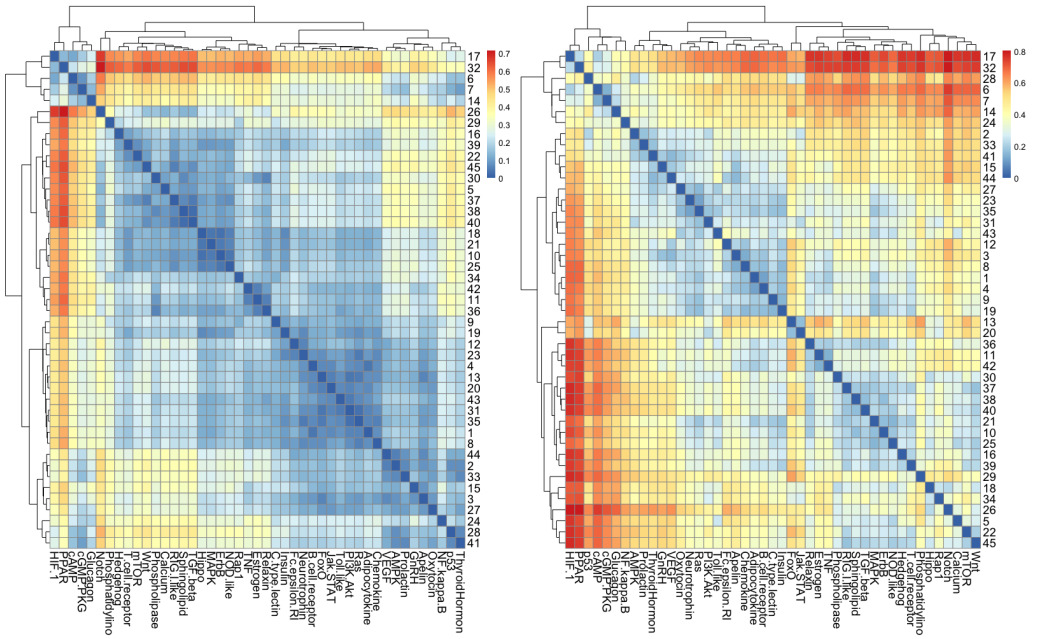

Figure 7 **The heatmap of H_{JS} distance computed for STN: (A) three-node subgraphs and (B) four-node subgraphs, with blue and red denote the small and large value of H_{JS}, respectively. The number of each row denotes the network name (File S1).**

Full-size DOI: 10.7717/peerj.13137/fig-7

signaling (*Yamanaka et al., 2004*; *Xin et al., 2004*). In addition, owing to the cross-talk of these two pathways, novel, non-invasive therapies can be developed (*Nicholas et al., 2017*).

For the second pair of networks, both ErbB and Hippo signaling pathways are regulated by circular RNA and microRNA in hypopharyngeal cancer (*Feng et al., 2019*). For the third pair of networks, it was demonstrated that the testis-specific protein Y-linked 1 (TSPY1) activates the PI3K/AKT and RAS signaling pathways by suppressing IGFBP3 expression in lung adenocarcinoma and liver hepatocellular carcinoma progression (*Tu et al., 2019*). By inhibiting the EGFR/AKT pathway in oral cancer, quercetin appears to be an effective anti-tumor agent (*Chan et al., 2016*).

Figure 6B depicts the plot of the normalized frequency distributions of the 4-node subgraphs. Again, only the first 30 patterns are shown. The difference between the "neurotrophin signaling pathway" and the "Ras signaling pathway" (green) distribution is minimal among the following subgraphs: id_78 and id_204, whereas the difference between the "adipocytokine signaling pathway" (blue) and "B-cell receptor signaling pathway" (purple) is minimal among the following subgraphs: id_78, id_204, id_328, id_330, and id_2184 (not shown in Fig. 6B).

The results of cluster analysis for STN are given in Figs. 7A and 7B.

From Figs. 7A and 7B, we noted that certain areas are associated with similar colors. The result suggests a group of STN possess similar subgraph topology.

Table 5 The top three most similar pairs of cellular processes based on the H_{JS} distance of the three-node subgraphs and four-node subgraphs.

Network A	Network B	H_{JS} distance	Absolute value of the difference of the subgraph normalized frequency distributions
	3-node subgraph ID		(ID 6, ID 12, ID 36, ID 38)
Cell-cycle	Cellular senescence	0.0697	(0.015, 0.078, 0.090, 0.004)
Apoptosis	Focal adhesion	0.0839	(0.095, 0.037, 0.041, 0.015)
Cellular senescence	Focal adhesion	0.106	(0.059, 0.098, 0.002, 0.034)
	4-node subgraph ID		(ID 14, ID 28, ID 74, ID 76, ID 78, ID 280, ID 328, ID 392, ID 2184)
Cell-cycle	Cellular senescence	0.125	(0.003, 0.0002, 0.001, 0.027, 0.001, 0.004, 0.057, 0.035, 0.039)
Apoptosis	Focal adhesion	0.143	(0.048, 0.013, 0.005, 0.041, 0.004, 0.023, 0.032, 0.016, 0.047)
Cell-cycle	Focal adhesion	0.205	(0.034, 0.047, 0.035, 0.008, 0.010, 0.083, 0.028, 0.054, 0.024)

Cellular processes

A list of the top three most similar H_{JS} distances for cellular processes is given in Table 5. The range of difference of the three-node subgraph distributions for the "cell cycle" and "cellular senescence" networks is 0.004–0.090, which is lower than that of the other two pairs of networks. The range of difference of the four-node subgraph distributions for the "cell cycle" and "cellular senescence" networks is 0.0002–0.0057, which is smaller than that of the other two pairs of networks. Once again, the results suggested that the underlying modular structure of molecular networks is dominated by irreducible subgraphs. The complete list of the H_{JS} distances of the cellular processes is given in File S7.

It is obvious that in Fig. 8A, the red and green dots are located close to each other for id_6 and id_38; this indicated that the H_{JS} distance between the "cell cycle" and the "cellular senescence" processes is minimal. The blue and purple dots are located close to each other for FFL (id_38), which suggests that the H_{JS} distance between the "apoptosis" and "focal adhesion" processes is small.

Biological interpretation—cellular processes

For the three-node case, the cellular senescence phenomenon (*Sun, Coppe & Lam, 2018*) is highly relevant to the cell-cycle process. Most of the drugs with anti-cancer potential are inducing cell-cycle arrest (*Hsu & Chung, 2012*; *Czarnomysy et al., 2018*) and apoptosis (*Lee et al., 2017*; *Liu et al., 2019*). Cellular senescence is a phenomenon that is characterized by irreversible cell-cycle arrest (*Sun, Coppe & Lam, 2018*), and it results from the coordination of cell-cycle arrest and cell expansion (*Ogrodnik et al., 2019*).

For the second pair of networks, numerous studies have shown the regulatory relationship between focal adhesion and apoptosis. *Luo et al. (2018)* studied the effect of a green tea compound on the proliferation and apoptosis of breast cancer cells by inhibiting the focal adhesion kinase (FAK) signaling pathway. FAK is an important component in regulating endothelial cell apoptosis (*Suhr & Bloch, 2012*). Cance and Golubovskaya

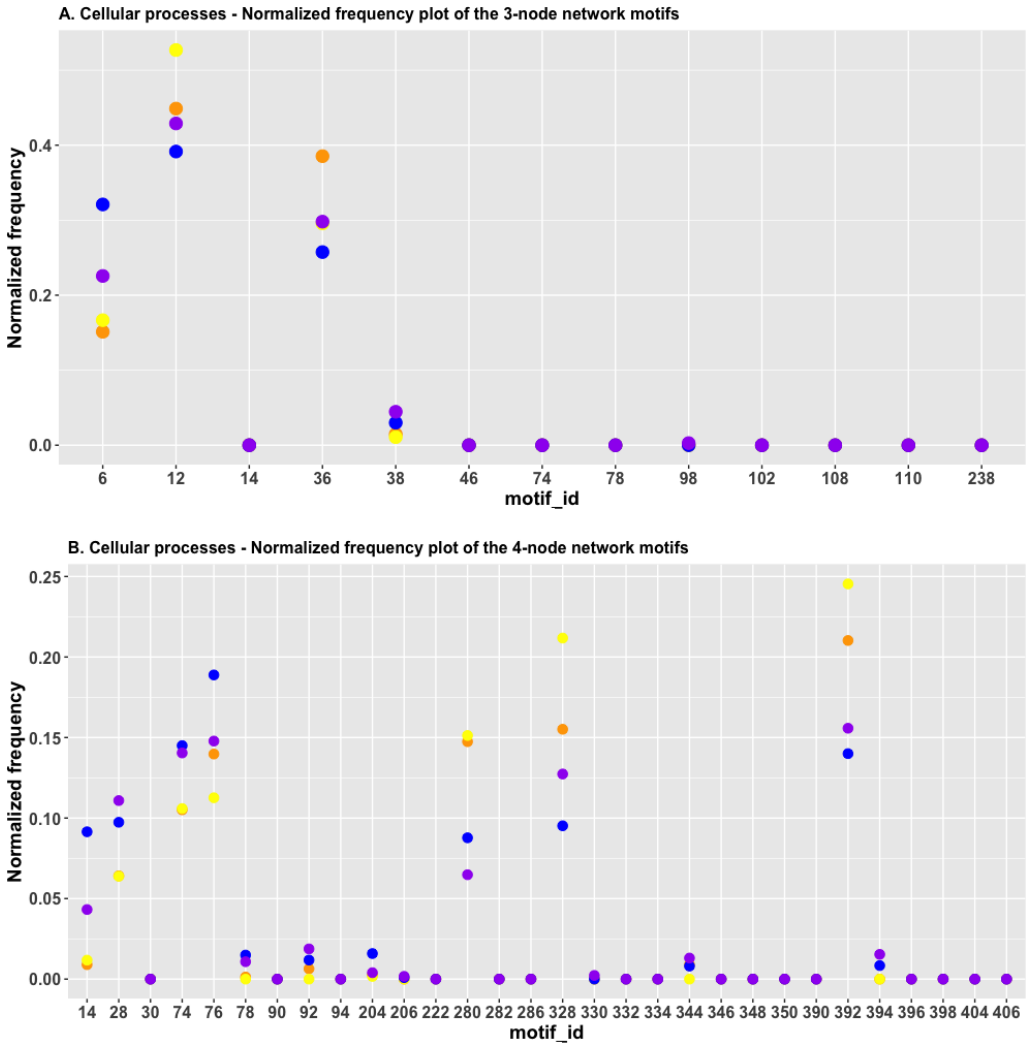

Figure 8 **(A) The plot of the normalized frequency of the three-node subgraphs for three pairs of cellular processes with the smallest H_{JS} distance. Color labelling of the cellular processes: cell cycle (orange), cellular senescence (yellow), apoptosis (blue), and focal adhesion (purple). (B) The plot of the normalized frequency distributions of the four-node subgraphs for three pairs of cellular processes with the smallest H_{JS} distance. Color labelling of the cellular processes are: cell cycle (orange), cellular senescence (yellow), apoptosis (blue) and focal adhesion (purple).**

Full-size DOI: 10.7717/peerj.13137/fig-8

reported that the interaction of FAK and p53 may promote cell survival or induce cell apoptosis (*Cance & Golubovskaya, 2008*).

For the third pair of networks, it was found that caveolin-1 suppresses FAK activity and triggers morphological alterations of the cell, changes enzyme activities and gene expression (*Park, 2017*; *Cho et al., 2004*), and that the inhibition of FAK expression can activate the cellular senescence program (*Chuang et al., 2019*).

Figure 8B depicts the plot of the normalized frequency distributions of the four-node subgraphs for cellular processes. Again, only the first 30 patterns are shown. The difference between the "cell cycle" (red) and "cellular senescence" (green) distributions is minimal

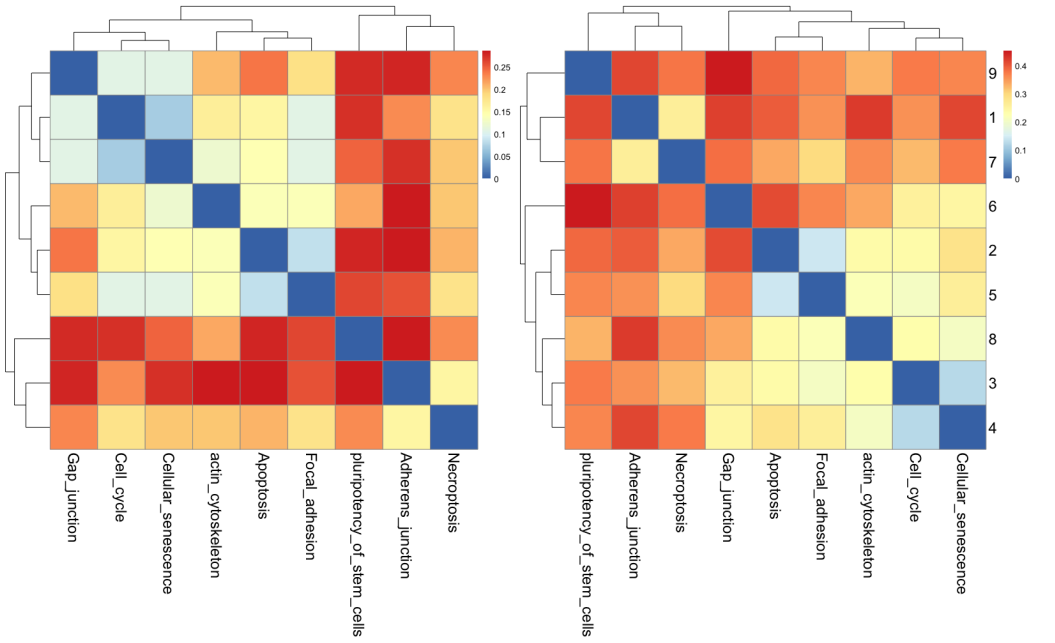

Figure 9 The heatmap of H_{JS} distance computed for cellular processes: (a) three-node subgraphs and (b) four-node subgraphs, with light yellow and darker red denote a small and large value of H_{JS} respectively. The number of each row denotes the network name (File S1).

Full-size DOI: 10.7717/peerj.13137/fig-9

among the following subgraphs: id_14, id_28, id_74, id_78, id_204 (0.001, not shown in Table 5), and id_280, whereas the difference between "apoptosis" (blue) and "focal adhesion" (purple) is minimal among the following subgraphs: id_74, id_78, id_92, id_206, id_330, and id_344 (the last four IDs are not shown in Table 5, and the normalized frequency magnitudes associated with them are small). For the third pair, the difference between "cell cycle" (red) and "focal adhesion" (purple) is minimal among the following subgraphs: id_76, id_78, id_204, id_206, id_330, and id_344 (the last four IDs are not shown in Table 5, and the normalized frequency magnitudes associated with them are small).

The results of cluster analysis for the cellular processes are given in Figs. 9A and 9B.

From Fig. 9A, the three-node subgraph clustering results, we identified the following pairs of highly similar networks: (i) "cell cycle" and "cellular senescence" and (ii) "apoptosis" and "focal adhesion". The results for the identified pairs of networks are consistent with the findings in Table 5.

For the four-node subgraphs, *i.e.*, Fig. 9B, the following highly similar pairs are detected: (i) "cell cycle" and "cellular senescence" and (ii) "apoptosis" and "focal adhesion". Moreover, the results of the identified pairs of networks are consistent with the findings listed in Table 5.

We also studied the inter-quartile range and median value of the H_{JS} distances of the cancer networks, STN and cellular processes; the results are given in File S8.

CONCLUSIONS

We studied the problem of determining the similarity of two directed networks by proposing an effective approach, the subgraph-based approach. First, the normalized frequency distributions of the three-node subgraphs and four-node subgraphs for three major types of molecular networks were calculated by using our algorithm, *PatternFinder*. Compared to other algorithms, *i.e. LoTo* and *acc-Motif*; our subgraph detection algorithm obtained similar results but had certain advantages.

Second, we conducted three simulation experiments, which confirmed the superiority of our method. The simulation experiments considered six network models along with three different network sizes and two edge densities. The accuracy of classification based on subgraph-based approach with information-theoretic entropy (H_{JS}) is 100%, which is better than the current status of other works.

Third, we used H_{JS} to infer pairs of networks that exhibit similar/different regulatory interaction topologies. In particular, our results suggested that there are common regulation modules for AML and pancreatic cancer formation. To the best of our knowledge, the present study is the first to combine the network subgraph concept and H_{JS} to address the molecular network similarity problem.

Fourth, we found that the underlying substructures of the molecular networks are dominated by irreducible subgraphs. This behavior holds true for the three classes of molecular networks we studied.

This study provides a systematic approach to dissect the underlying structures of molecular networks. We hypothesize that network structures can be understood in terms of the network subgraphs.

In future, the next step is to test our hypothesis by conducting five-node subgraphs analysis. As a first step towards five-node subgraph analysis, we have published papers on how to generate all the five-node subgraphs (*Efendi Zaenudin et al., 2019*). Regarding the applications of the five-node subgraph study, we plan to examine the association of the five-node subgraph modules and driver genes for cancer networks. Cancer driver genes are genes that give selective advantage for cancer progression. The level of association/enrichment is given by using odds ratio (OR). An OR >1 indicates that driver genes are enriched in the subgraph module. In our previous work (*Huang et al., 2020*), we examined the association of both the three-node and four-node subgraph modules and driver genes, and have found that many cancer networks, STN, cellular processes have an OR > 1. Similarity, we also have investigated the association of the subgraph module and essential genes (*Efendi, Huang & Ng, 2021*), but there are only a few networks enriched with essential genes. In conclusion, we have proposed a novel and effective approach, subgraph-based method, to compare and classify molecular networks with diverse functionalities.

ACKNOWLEDGEMENTS

We would like to thank Mr. Ci-Jun Peng and Mr. I-Lun Hsieh, who spent efforts on developing the codes. We also thank the 'Editage Professional English Editing Service, Cactus Communications', for editing the English.

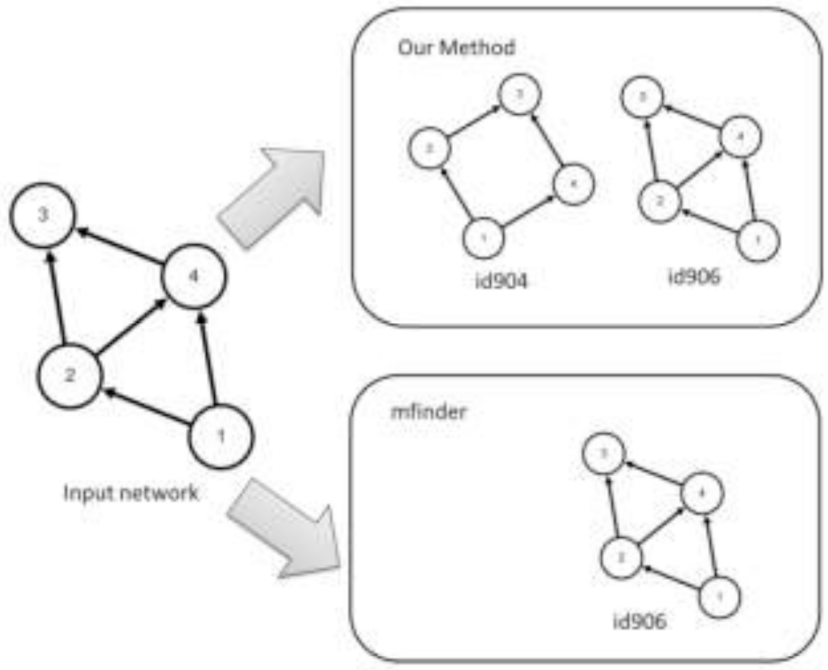

Figure A1 **A comparison of two identification algorithms: *mfinder* and *PatternFinder*.**
Full-size DOI: 10.7717/peerj.13137/fig-10

APPENDIX

Subgraph identification tool—the *PatternFinder* algorithm

Many network motif detection tools have been developed to detect network motifs; including: FANMOD, MAVISTO, MFINDER, NetMatch, and SNAVI. We have reported (*Hsieh et al., 2015*) that those tools have at least two limitations: (i) motifs identified in one round may not be recoverable in another round because of the use of randomized algorithm, and (ii) nodes identities are missing.

We developed an algorithm named *PatternFinder* (*Huang et al., 2020*; *Lee, 2016*) to identify: (i) both three-node and four-node subgraphs in a network, and (ii) functional subgraphs embedded in the three-node subgraphs and four-node subgraphs not identified by MFINDER. We refer the reader to reference *Lee (2016)* for a more detail description of *PatternFinder*. Below we briefly summarized the *PatternFinder* algorithm.

Given the ”Input network”, *PatternFinder* is able to identify two four-node subgraphs, *i.e.*, the subgraph ‘id_904’ and subgraph ‘id_906’, whereas MFINDER can identify the subgraph ‘id_906’ only (Fig. A1). MFINDER considers motif ‘id_904’ is an independent subgraph. *PatternFinder* is able to identify subgraphs embedded in a subgraph.

In the following, a four-node subgraph is used as an example to illustrate the basic concept behind the *PatternFinder* algorithm. Given a network called ‘*net*’ composes of 20 nodes, an adjacency matrix can be constructed. Let n denotes the total number of nodes. Assuming that we want to identify a subgraph, denoted by ‘id_2204’, *PatternFinder* read in the ‘2204’ pattern. This subgraph composes of four nodes and five edges, where the

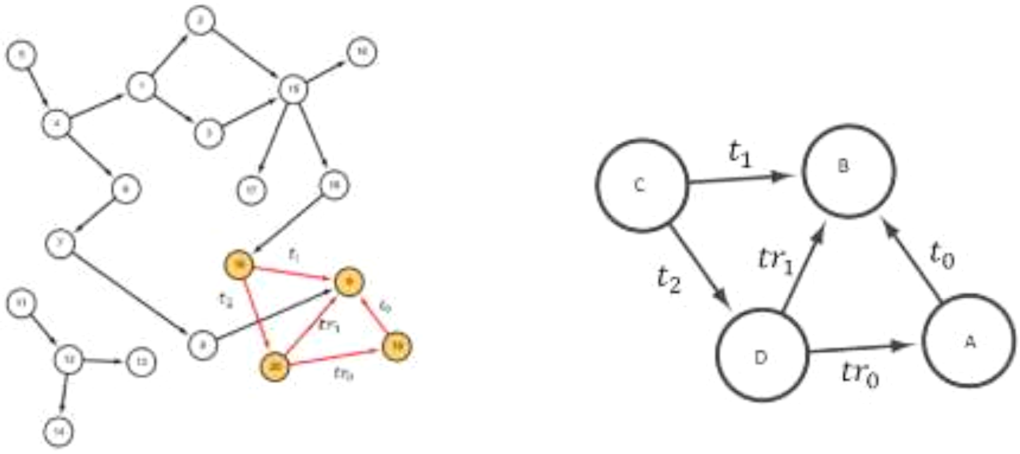

Figure A2 **(A) An input network named '*net*' and (B) the four-node subgraph 'id_2204'.**
Full-size DOI: 10.7717/peerj.13137/fig-11

edges are denoted by $\boldsymbol{t}_0$, $\boldsymbol{t}_1$, $\boldsymbol{t}_2$, $\boldsymbol{tr}_0$ and $\boldsymbol{tr}_1$. Starting from node A, *PatternFinder* begins to examine the following patterns: (i) is node A and node B connects with an edge $\boldsymbol{t}_0$, (ii) is node B and node C connects with an edge $\boldsymbol{t}_1$, (iii) is node C and node D connects with an edge $\boldsymbol{t}_2$, and (iv) is node D and node A connects with an edge t_0, and node D and node B connects with an edge $\boldsymbol{tr}_1$.

Starting from the network named '*net*', the algorithm begins the search from node 1 and labels it as node A. Node 1 and node 2 or node B are linked, the edge is denoted by *edge* (1, 2). The algorithm continues to search if there is a node links to node B, if not, the algorithm will relabel node B to node 3 and repeat the search. From Fig. A2, it was found that $A = 19$, $B = 9$, $C = 10$, and $D = 20$ are connected by three edges, *i.e.*, *edge* (19,9) $= \boldsymbol{t}_0$, *edge* (9,10) $= \boldsymbol{t}_1$, *edge* (10,20) $= \boldsymbol{t}_2$, hence, four nodes are identified. However, according to the subgraph 'id_2204', there are two more edges which need to be determined, *i.e.*, *edge* (20,9) $= \boldsymbol{tr}_1$ and *edge* (20,19) $= \boldsymbol{tr}_2$. The computation time complexity of the algorithm *PatternFinder* is $O(n^4)$.

ADDITIONAL INFORMATION AND DECLARATIONS

Funding

The work of Chien-Hung Huang is supported by the grant of the Ministry of Science and Technology of Taiwan (MOST) (grant number MOST 109-2221-E-150-036). Dr. Ka-Lok Ng and Efendi Zaenudin works are supported by the MOST (grant numbers MOST 109-2221-E-468-013 and MOST 108-2221-E-468-020) and grants from Asia University (grant number ASIA-110-CMUH-12). The funders had no role in study design, data collection and analysis, decision to publish, or preparation of the manuscript.

Grant Disclosures

The following grant information was disclosed by the authors:
Ministry of Science and Technology of Taiwan (MOST): MOST 109-2221-E-150-036.
MOST: MOST 109-2221-E-468-013, MOST 108-2221-E-468-020.

Competing Interests

The authors declare there are no competing interests.

Author Contributions

- Chien-Hung Huang and Ka-Lok Ng conceived and designed the experiments, performed the experiments, analyzed the data, prepared figures and/or tables, authored or reviewed drafts of the paper, and approved the final draft.
- Efendi Zaenudin performed the experiments, analyzed the data, prepared figures and/or tables, authored or reviewed drafts of the paper, and approved the final draft.
- Jeffrey J.P. Tsai conceived and designed the experiments, authored or reviewed drafts of the paper, managed the project and secured the necessary acquisition funding, and approved the final draft.
- Nilubon Kurubanjerdjit performed the experiments, prepared figures and/or tables, and approved the final draft.

Data Availability

The following information was supplied regarding data availability:

The raw data is available in the Supplementary Files.

Supplemental Information

Supplemental information for this article can be found online at http://dx.doi.org/10.7717/peerj.13137#supplemental-information.

REFERENCES

Aparìcio DO, Ribeiro PMP, Silva FMA. 2015. Network comparison using directed graphlets. ArXiv preprint. arXiv:1511.01964.

Arakelyan A, Nersisyan L. 2013. KEGGParser: parsing and editing KEGG pathway maps in Matlab. *Bioinformatics* **29(4)**:518–519 DOI 10.1093/bioinformatics/bts730.

Arefin AS, Vimieiro R, Riveros C, Craig H, Moscato P. 2014. An information theoretic clustering approach for unveiling authorship affinities in Shakespearean era plays and poems. *PLOS ONE* **9(10)**:e111445 DOI 10.1371/journal.pone.0111445.

Bagrow JP, Bollt EM. 2019. An information-theoretic, all-scales approach to comparing networks. *Applied Network Science* **4**:1–15 DOI 10.1007/s41109-018-0108-x.

Burack WR, Shaw AS. 2000. Signal transduction: hanging on a scaffold. *Current Opinion in Cell Biology* **12(2)**:211–216 DOI 10.1016/S0955-0674(99)00078-2.

Butala A, Kalra J, Rosner F. 1989. Chronic myelocytic leukemia and gastric cancer in the same patient. *Journal of the National Medical Association* **81(4)**:457–459.

Cance WG, Golubovskaya VM. 2008. Focal adhesion kinase versus p53: apoptosis or survival? *Science Signaling* **1(20)**:pe22.

Capra JA, Singh M. 2007. Predicting functionally important residues from sequence conservation. *Bioinformatics* **23(15)**:1875–1882 DOI 10.1093/bioinformatics/btm270.

Cascetta K, Meier DE, Tracy B, Gruenstein S, Cascetta K. 2014. A 60-year-old male with synchronous acute myeloid leukemia and metastatic adenocarcinoma of the pancreas. *Seminars in Oncology* **41**:e51–e59 DOI 10.1053/j.seminoncol.2014.09.023.

Chan CY, Lien C-H, Lee M-F, Huang C-Y. 2016. Quercetin suppresses cellular migration and invasion in human head and neck squamous cell carcinoma (HNSCC). *Biomedicine* **6(3)**:10–15 DOI 10.7603/s40681-016-0015-3.

Chen P-D, Chen C-N, Hu R-H, Lai H-S. 2017. Clinical experience of double primary gastric cancer and hepatocellular carcinoma. *Formosan Journal of Surgery* **50(1)**:10–15 DOI 10.4103/fjs.fjs_9_17.

Cho K, Ryu SJ, Oh YS, Park JH, Lee JW, Kim H-P, Kim KT, Jang IS, Park SC. 2004. Morphological adjustment of senescent cells by modulating Caveolin-1 status. *The Journal of Biological Chemistry* **279**:42270–42278 DOI 10.1074/jbc.M402352200.

Chuang HH, Wang P-H, Niu S-W, Zhen Y-Y, Huang M-S, Hsiao M, Yang C-J. 2019. Inhibition of FAK signaling elicits lamin A/C-associated nuclear deformity and cellular senescence. *Frontiers in Oncology* **9**:22 DOI 10.3389/fonc.2019.00022.

Csardi G, Nepusz T. 2006. The igraph software package for complex network research. *InterJournal, Complex Systems* **5**:1–9.

Czarnomysy R, Surazyński A, Muszynska A, Gornowicz A, Bielawska A, Bielawski K. 2018. A novel series of pyrazole-platinum(II) complexes as potential anticancer agents that induce cell cycle arrest and apoptosis in breast cancer cells. *Journal of Enzyme Inhibition and Medicinal Chemistry* **33(1)**:1006–1023 DOI 10.1080/14756366.2018.1471687.

De Castro JA, Vencer L, Espinosa W. 2017. Acute myelogenous leukemia presenting as acute pancreatitis: a case of primary pancreatic extramedullary acute myeloid leukemia. *Clinical Gastroenterology and Hepatology* **15(1)**:e30–e31.

Dennler S, Goumans MJ, Ten Dijke P. 2002. Transforming growth factor beta signal transduction. *Journal of Leukocyte Biology* **71(5)**:731–740.

Efendi Z, Huang CH, Ng KL. 2021. Identifying network subgraph-associated essential genes in molecular networks using a network subgraph approach. *International Journal of Mathematical and Computational Sciences* **15(5)**:71–77.

Efendi Zaenudin EBW, Dessie EY, Reddy MV, Tsai JJP, Huang C-H, Ng K-L. 2019. A parallel algorithm to generate connected network motifs. *IAENG International Journal of Computer Science* **46(4)**:518–523.

Endres D, Schindelin J. 2003. A new metric for probability distributions. *Information Theory, IEEE Transactions* **49**:1858–1860 DOI 10.1109/TIT.2003.813506.

Feng C, Li Y, Lin Y, Cao X, Li D, Zhang H, He X. 2019. CircRNA-associated ceRNA network reveals ErbB and Hippo signaling pathways in hypopharyngeal cancer. *International Journal of Molecular Medicine* **43(1)**:127–142.

Gao S, Hu X-D, Wang S-Z, Liu N, Zhao W, Yu Q-X, Hou W-H, Yuan S-H. 2015. Gastric metastasis from small cell lung cancer: a case report. *World Journal of Gastroenterology* **21(5)**:1684–1688 DOI 10.3748/wjg.v21.i5.1684.

Grosse I, Bernaola-Galván P, Carpena P, Román-Roldán R, Oliver J, Stanley HE. 2002. Analysis of symbolic sequences using the Jensen–Shannon divergence. *Physical review. E, Statistical, Nonlinear, and Soft Matter Physics* **65(4 Pt 1)**:041905 DOI 10.1103/PhysRevE.65.041905.

Gültas M, Düzgün G, Herzog S, Jäger SJ, Meckbach C, Wingender E, Waack S. 2014. Quantum coupled mutation finder: predicting functionally or structurally important sites in proteins using quantum Jensen–Shannon divergence and CUDA programming. *BMC Bioinformatics* **15(1)**:96 DOI 10.1186/1471-2105-15-96.

Heymans M, Singh AK. 2003. Deriving phylogenetic trees from the similarity analysis of metabolic pathways. *Bioinformatics* **19(suppl_1)**:i138–i146 DOI 10.1093/bioinformatics/btg1018.

Hsieh WT, Tzeng KR, Ciou JS, Tsai JJP, Kurubanjerdjit N, Huang CH, Ng K-L. 2015. Transcription factor and microRNA-regulated network motifs for cancer and signal transduction networks. *BMC Systems Biology* **9(1)**:S5.

Hsu SC, Chung JG. 2012. Anticancer potential of emodin. *Biomedicine* **2(3)**:108–116 DOI 10.1016/j.biomed.2012.03.003.

Hu Z-R, Huang C-T, Chen W-Y, Wu H-C, Kuo Y-H, Li C-F, Chang S-J, Feng Y-H. 2014. Synchronous gastric cancer and hepatocellular carcinoma. *Journal of Cancer Research and Practice* **1(3)**:226–232.

Huang CY, Ju D-T, Chang C-F, Muralidhar Reddy P, Velmurugan BK. 2017. A review on the effects of current chemotherapy drugs and natural agents in treating non-small cell lung cancer. *Biomedicine* **7(4)**:23 DOI 10.1051/bmdcn/2017070423.

Huang CH, Zaenudin E, Tsai JJP, Kurubanjerdjit N, Dessie EY, Ng K-L. 2020. Dissecting molecular network structures using a network subgraph approach. *PeerJ* **8**:e9556 DOI 10.7717/peerj.9556.

Jung Y-S, Park J-I. 2020. Wnt signaling in cancer: therapeutic targeting of Wnt signaling beyond β-catenin and the destruction complex. *Experimental & Molecular Medicine* **52(2)**:183–191 DOI 10.1038/s12276-020-0380-6.

Kiani NA, Zenil H, Olczak J, Tegnér J. 2016. Evaluating network inference methods in terms of their ability to preserve the topology and complexity of genetic networks. *Seminars in Cell & Developmental Biology* **51**:44–52 DOI 10.1016/j.semcdb.2016.01.012.

Kim JY, Kim YY, Kim SJ, Park JC, Kwon YH, Jung MK, Kwon OK, Chung HY, Yu W, Park JY, Lee YK, Park SS, Jeon SW. 2013. Predictive factors for lymph node metastasis in signet ring cell gastric cancer and the feasibility of endoscopic submucosal dissection. *Journal of Gastric Cancer* **13(2)**:93–97 DOI 10.5230/jgc.2013.13.2.93.

Koch S. 2021. Regulation of Wnt signaling by FOX transcription factors in cancer. *Cancers* **13(14)**:3446 DOI 10.3390/cancers13143446.

Koh SA, Lee KH. 2014. Adenocarcinoma of lung cancer with solitary metastasis to the stomach. *The Korean Journal of Gastroenterology* **64(3)**:154–157 DOI 10.4166/kjg.2014.64.3.154.

Krishnamurthy N, Kurzrock R. 2018. Targeting the Wnt/beta-catenin pathway in cancer: update on effectors and inhibitors. *Cancer Treatment Reviews* **62**:50–60 DOI 10.1016/j.ctrv.2017.11.002.

Kugler KG, Mueller LAJ, Graber A, Dehmer M. 2011. Integrative network biology: graph prototyping for co-expression cancer networks. *PLOS ONE* **6(7)**:e22843 DOI 10.1371/journal.pone.0022843.

Lee HX. 2016. In silico study of significant network motifs in the cancer networks. Master Thesis, National Formosa University, Taiwan. Advisor: Huang CH, co-advisor: Ng KL.

Lee MR, Lin C, Lu C-C, Kuo S-C, Tsao J-W, Juan Y-N, Chiu H-Y, Lee F-Y, Yang J-S, Tsai F-J. 2017. YC-1 induces G(0)/G(1) phase arrest and mitochondria-dependent apoptosis in cisplatin-resistant human oral cancer CAR cells. *Biomedicine* **7(2)**:31–42 DOI 10.1051/bmdcn/2017070205.

Li X, Li S, Ma Z, Zhao S, Wang X, Wen D. 2018. Multiple gastrointestinal metastases of squamous-cell lung cancer: a case report. *Medicine* **97(24)**:e11027 DOI 10.1097/MD.0000000000011027.

Liu L, Fan J, Ai G, Liu J, Luo N, Li C, Cheng Z. 2019. Berberine in combination with cisplatin induces necroptosis and apoptosis in ovarian cancer cells. *Biological Research* **52(1)**:37 DOI 10.1186/s40659-019-0243-6.

Loog M, Wessels L, Reinders MJT, De Ridder D (eds.) 2011. Pattern recognition in bioinformatics. In: *6th IAPR international conference, PRIB 2011 Delft, The Netherlands, November 2-4, 2011 Proceedings*. Springer-Verlag Berlin Heidelberg.

Luo X, Guo L, Zhang L, Hu Y, Shang D, Ji D. 2018. Bioinformatics analysis of microarray profiling identifies the mechanism of focal adhesion kinase signalling pathway in proliferation and apoptosis of breast cancer cells modulated by green tea polyphenol epigallocatechin 3-gallate. *Journal of Pharmacy and Pharmacology* **70(12)**:1606–1618 DOI 10.1111/jphp.13010.

Mangal M, Sudharsanan S, Elamurugan TP, Jagdish S. 2018. Gastric carcinoma in a patient with chronic lymphocytic leukemia: coincidence or consequence? *Cureus* **10(4)**:e2405.

Martin AJ, Contreras-Riquelme S, Dominguez C, Perez-Acle T. 2017. LoTo: a graphlet based method for the comparison of local topology between gene regulatory networks. *PeerJ* **5**:e3052 DOI 10.7717/peerj.3052.

Martin AJ, Dominguez C, Contreras-Riquelme S, Holmes DS, Perez-Acle T. 2016. Graphlet based metrics for the comparison of gene regulatory networks. *PLOS ONE* **11(10)**:e0163497 DOI 10.1371/journal.pone.0163497.

Meira L, Máximo VR, Fazenda Á, Conceição AFD. 2018. An faster network motif detection tool. ArXiv preprint. arXiv:1804.09741.

Meira LAA, Máximo VR, Fazenda ÁL, Da Conceição AF. 2014. Acc-Motif: accelerated network motif detection. *IEEE/ACM Transactions on Computational Biology and Bioinformatics* **11(5)**:853–862 DOI 10.1109/TCBB.2014.2321150.

Messager M, Amielh D, Chevallier C, Mariette C. 2012. Isolated granulocytic sarcoma of the pancreas: a tricky diagnostic for primary pancreatic extramedullary acute myeloid leukemia. *World Journal of Surgical Oncology* **10**:13 DOI 10.1186/1477-7819-10-13.

Mokhtarifard A, Kooshyar MM, Nassiri MR, Mohammadipour A, Edalatianalipour Z. 2016. Gastric cancer and CML: a literature review and case report. *WCRJ* **3(2)**:e709.

Mowshowitz A. 1968. Entropy and the complexity of graphs: II. The information content of digraphs and infinite graphs. *The Bulletin of Mathematical Biophysics* **30(2)**:225–240 DOI 10.1007/BF02476692.

Mowshowitz A, Mitsou V. 2009. Entropy, orbits, and spectra of graphs. In: *Analysis of complex networks*. Wiley-vch, 1–22. *Available at https://application.wiley-vch.de/books/sample/3527323457_c01.pdf* .

Nakaya A, Katayama T, Itoh M, Hiranuka K, Kawashima S, Moriya Y, Okuda S, Tanaka M, Tokimatsu T, Yamanishi Y, Yoshizawa AC, Kanehisa M, Goto S. 2013. KEGG OC: a large-scale automatic construction of taxonomy-based ortholog clusters. *Nucleic Acids Research* **41(Database issue)**:D353–D357.

Nicholas SE, Rowsey TG, Priyadarsini S, Mandal NA, Karamichos D. 2017. Unravelling the interplay of sphingolipids and TGF-beta signaling in the human corneal stroma. *PLOS ONE* **12(8)**:e0182390 DOI 10.1371/journal.pone.0182390.

Nishida K, Ono K, Kanaya S, Takahashi K. 2014. KEGGscape: a cytoscape app for pathway data integration. *F1000Research* **3**:144 DOI 10.12688/f1000research.4524.1.

Nitipir C, Ginghina O, Popa L, Andrei F, Tudor N, Radu I, Iaciu C, Orlov C, Vasilescu F, Balalau C, Leon G, Negrei C, Barbu MA. 2018. A rare case of advanced lung cancer presenting as a symptomatic gastric tumor. *Molecular and Clinical Oncology* **8(4)**:600–602.

Ogrodnik M, Salmonowicz H, Jurk D, Passos JF. 2019. Expansion and cell-cycle arrest: common denominators of cellular senescence. *Trends in Biochemical Sciences* **44(12)**:996–1008 DOI 10.1016/j.tibs.2019.06.011.

Omidi S, Schreiber F, Masoudi-Nejad A. 2009. MODA: an efficient algorithm for network motif discovery in biological networks. *Genes & Genetic Systems* **84(5)**:385–395 DOI 10.1266/ggs.84.385.

Park MK. 1998. A case of early gastric cancer associated with small cell lung cancer. *Journal of the Korean Cancer Association* **30(2)**:414–420.

Park SC. 2017. Survive or thrive: tradeoff strategy for cellular senescence. *Experimental & Molecular Medicine* **49(6)**:e342–e342 DOI 10.1038/emm.2017.94.

Pržulj N. 2007. Biological network comparison using graphlet degree distribution. *Bioinformatics* **23(2)**:e177–e183 DOI 10.1093/bioinformatics/btl301.

Sakumura M, Tajiri K, Sugiyama T. 2018. Gastric metastasis of hepatocellular carcinoma mimicking early gastric cancer. *Clinical Gastroenterology and Hepatology* **16(10)**:e99–e100 DOI 10.1016/j.cgh.2017.09.050.

Sano T, Tomaru K, Koide T, Masuda M, Yamamoto M, Miyazawa N, Inayama Y, Kaneko T, Ishigatsubo Y. 1986. A case report of synchronous small cell lung cancer and gastric cancer successfully treated with carboplatin. *Japanese Journal of Cancer Research* **77(8)**:790–798.

Sarajlić A, Malod-Dognin N, Yaveroğlu ÖN, Pržulj N. 2016. Graphlet-based characterization of directed networks. *Scientific Reports* **6(1)**:35098 DOI 10.1038/srep35098.

Schafer HS, Becker H, Schmitt-Gräff A, Lbbert M. 2008. Granulocytic sarcoma of Core-binding Factor (CBF) acute myeloid leukemia mimicking pancreatic cancer. *Leukemia Research* **32(9)**:1472–1475 DOI 10.1016/j.leukres.2008.02.017.

Snyder EL, Watanabe H, Magendantz M, Hoersch S, Chen TA, Wang DG, Crowley D, Whittaker CA, Meyerson M, Kimura S, Jacks T. 2013. Nkx2-1 represses a latent gastric differentiation program in lung adenocarcinoma. *Molecular Cell* **50(2)**:185–199 DOI 10.1016/j.molcel.2013.02.018.

Suhr F, Bloch W. 2012. Endothelial cell apoptosis: a new focal adhesion assembly makes the difference. *Circulation Research* **111(12)**:1488–1490 DOI 10.1161/CIRCRESAHA.112.278713.

Sun Y, Coppe JP, Lam EW. 2018. Cellular senescence: the sought or the unwanted? *Trends in Molecular Medicine* **24(10)**:871–885 DOI 10.1016/j.molmed.2018.08.002.

Tantardini M, Ieva F, Tajoli L, Piccardi C. 2019. Comparing methods for comparing networks. *Scientific Reports* **9(1)**:17557 DOI 10.1038/s41598-019-53708-y.

Tawada A, Chiba T, Ooka Y, Yokota H, Kanogawa N, Motoyama T, Saito T, Ogasawara S, Suzuki E, Hanari N, Matsubara H, Saeki N, Kambe M, Kishimoto T, Nakatani Y, Yokosuka O. 2014. Intracranial metastasis in a patient with hepatocellular carcinoma and gastric cancer. *Case Reports in Oncology* **7(1)**:199–203 DOI 10.1159/000360982.

Tran NT, Mohan S, Xu Z, Huang C-H. 2015. Current innovations and future challenges of network motif detection. *Briefings in Bioinformatics* **16(3)**:497–525 DOI 10.1093/bib/bbu021.

Trpevski I, Malod-Dognin N, Yaveroğlu ÖN, Pržulj N. 2016. Graphlet characteristics in directed networks. *Scientific Report* **6**:37057 DOI 10.1038/srep37057.

Tu W, Yang B, Leng X, Pei X, Xu J, Liu M, Dong Q, Tao D, Lu Y, Liu Y, Yang Y. 2019. Testis-specific protein, Y-linked 1 activates PI3K/AKT and RAS signaling pathways through suppressing IGFBP3 expression during tumor progression. *Cancer Science* **110(5)**:1573–1586 DOI 10.1111/cas.13984.

Uenishi T, Kubo S, Hirohashi K, Osugi H, Shuto T, Tanaka H, Yamamoto T, Ogawa M, Kinoshita H. 2003. Surgical management of synchronous hepatocellular carcinoma and gastric cancer. *Digestive Surgery* **20(2)**:133–140 DOI 10.1159/000069389.

Wernicke S, Rasche F. 2006. FANMOD: a tool for fast network motif detection. *Bioinformatics* **22(9)**:1152–1153 DOI 10.1093/bioinformatics/btl038.

Wong A, You M. 1985. Entropy and distance of random graphs with application to structural pattern recognition. In: *Pattern analysis and machine intelligence, IEEE Transactions. PAMI-7*. 599–609.

Xin C, Ren S, Kleuser B, Shabahang S, Eberhardt W, Radeke H, Schäfer-Korting M, Pfeilschifter J, Huwiler A. 2004. Sphingosine 1-phosphate cross-activates the Smad signaling cascade and mimics transforming growth factor-beta-induced cell responses. *Journal of Biological Chemistry* **279(34)**:35255–35262 DOI 10.1074/jbc.M312091200.

Yamanaka M, Shegogue D, Pei H, Bu S, Bielawska A, Bielawski J, Pettus B, Hannun YA, Obeid L, Trojanowska M. 2004. Sphingosine kinase 1 (SPHK1) is induced by transforming growth factor-beta and mediates TIMP-1 up-regulation. *Journal of Biological Chemistry* **279(52)**:53994–54001 DOI 10.1074/jbc.M410144200.

Yang M-D, Lin K-C, Lu M-C, Jeng L-B, Hsiao C-L, Yueh T-C, Fu C-K, Li H-T, Yen S-T, Lin C-W, Wu C-W, Pang S-Y, Bau D-T, Tsai F-J. 2017. Contribution of matrix metalloproteinases-1 genotypes to gastric cancer susceptibility in Taiwan. *BioMedicine* **7(2)**:10–10 DOI 10.1051/bmdcn/2017070203.

Yaveroglu ON, Malod-Dognin N, Davis D, Levnajic Z, Janjic V, Karapandza R, Stojmirovic A, Pržulj N. 2014. Revealing the hidden language of complex networks. *Scientific Report* **4**:4547.

Yaveroğlu ÖN, Milenković T, Pržulj N. 2015. Proper evaluation of alignment-free network comparison methods. *Bioinformatics* **31(16)**:2697–2704 DOI 10.1093/bioinformatics/btv170.

Zenil H, Kiani NA, Tegnér J. 2013. Algorithmic complexity of motifs clusters super-families of networks. In: *2013 IEEE international conference on bioinformatics and biomedicine*.

Zenil H, Kiani NA, Tegnér J. 2015. Quantifying loss of information in network-based dimensionality reduction techniques. *Journal of Complex Networks* **4(3)**:342–362.

Zhu D, Qin ZS. 2005. Structural comparison of metabolic networks in selected single cell organisms. *BMC Bioinformatics* **6(1)**:8 DOI 10.1186/1471-2105-6-8.